IOP Publishing Smart Materials and Structures
Smart Mater. Struct. **26** (2017) 085040 (13pp) https://doi.org/10.1088/1361-665X/aa7a4e

Accurately controlled sequential self-folding structures by polystyrene film

Dongping Deng[1], Yang Yang[1], Yong Chen[1,], Xing Lan[2] and Jesse Tice[2]

[1] Daniel J Epstein Department of Industrial and Systems Engineering, University of Southern California, Los Angeles, CA 90089, United States of America
[2] NG Next, Northrop Grumman Corporation, Redondo Beach, CA 90278, United States of America

E-mail: yongchen@usc.edu

Received 15 March 2017, revised 7 June 2017
Accepted for publication 19 June 2017
Published 28 July 2017

Abstract

Four-dimensional (4D) printing overcomes the traditional fabrication limitations by designing heterogeneous materials to enable the printed structures evolve over time (the fourth dimension) under external stimuli. Here, we present a simple 4D printing of self-folding structures that can be sequentially and accurately folded. When heated above their glass transition temperature pre-strained polystyrene films shrink along the *XY* plane. In our process silver ink traces printed on the film are used to provide heat stimuli by conducting current to trigger the self-folding behavior. The parameters affecting the folding process are studied and discussed. Sequential folding and accurately controlled folding angles are achieved by using printed ink traces and angle lock design. Theoretical analyses are done to guide the design of the folding processes. Programmable structures such as a lock and a three-dimensional antenna are achieved to test the feasibility and potential applications of this method. These self-folding structures change their shapes after fabrication under controlled stimuli (electric current) and have potential applications in the fields of electronics, consumer devices, and robotics. Our design and fabrication method provides an easy way by using silver ink printed on polystyrene films to 4D print self-folding structures for electrically induced sequential folding with angular control.

Supplementary material for this article is available online

Keywords: sequential self folding, accurate controlled folding angle, 4D printing, electrically stimulate

(Some figures may appear in colour only in the online journal)

1. Introduction

Self-folding structures change the shape after fabrication under certain stimuli such as heat [1–3], moisture [4, 5], and solvent [6–8]. With the emergence of four-dimensional (4D) printing technology [9–12] these structures have received increased attention recently. Self-folding structures have enormous potential for micro devices [13–15], drug delivery systems [8, 16–18], reconfigurable systems [19–21] and folded circuit designs [22–24]. Instead of direct printing three-dimensional (3D) structures, 4D printing relies on introducing heterogeneous materials into a printed structure. Upon triggering by external stimuli, the energy is released and the structure evolves over time (the fourth dimension) to form desired 3D shapes. Various mechanisms have been developed to realize the 4D printing process, such as shape memory materials [25, 26], bilayer structures [27–29] and active hinge based structures [30, 31]. The design and fabrication complexity varies among these mechanisms. Prior research based on pre-strained polystyrene film used printed black ink to define the folding hinges, and used infrared light to raise the ink's temperature faster than the surrounding materials to create a thermal expansion difference to generate folding behavior [32]. Pre-strained polystyrene films have also been used as active materials in sandwiched structure design by coating with another passive material with designed patterns to achieve self-folding structures [33–35]. Since polystyrene films are responsive to heat, other heating sources have also

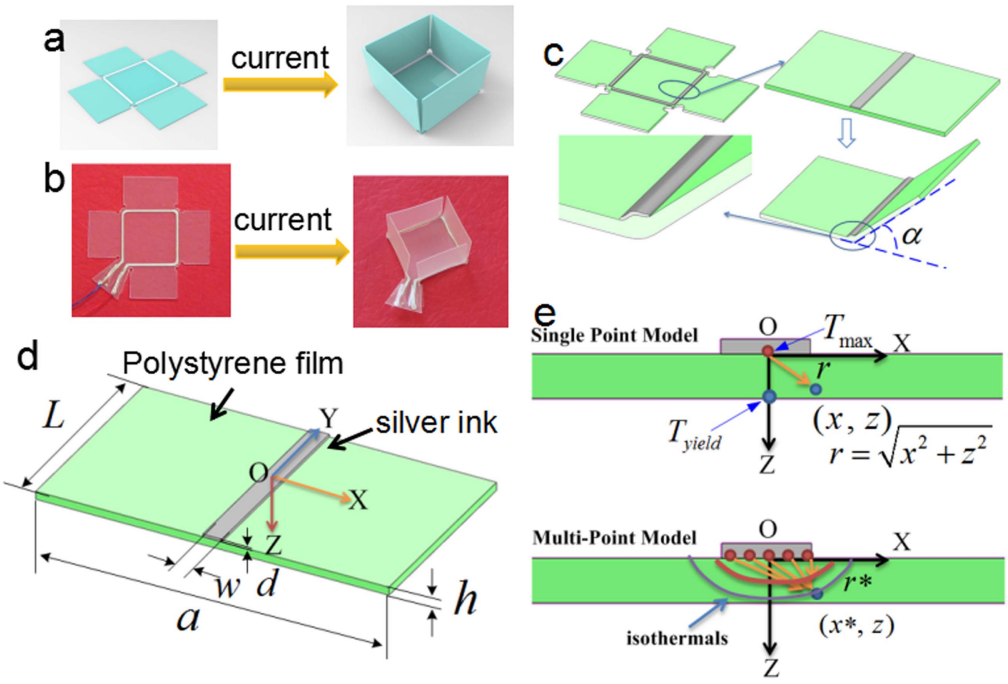

Figure 1. Principle of the self-folding structure. (a), (b) Schematic diagram and images of a self-folded cube; (c) modeling of the folding structure; (d) design parameters of the self-folding structure; and (e) thermal models.

been studied such as laser [36] and microwave [37]. Electrically induced self-folding is also studied with sandwiched structures by employing ink traces on layered laser cut copper films that are glued together [33]; however, the preparation of these structures are complex and cumbersome. Recently some sequential self-folding approaches have been studied, in which ink in various gray scale is printed on polystyrene films and sequential folding is achieved through a local light absorption approach [38] or using shape memory polymers [39, 40]. Similar approaches using hinges with varied folding conditions were demonstrated in 3D printed multiple-material objects [12]. However, the light exposure is a global stimuli; therefore each hinge cannot be separately controlled. Additionally, the light becomes shadowed during the folding process, which precludes local control throughout the process. Instead of light exposure, electrically induced self-folding provides design freedom to realize complex sequential folding due to its flexibility in providing controlled and local heating.

In this paper, we utilize an electrically induced self-folding method in which the self-folding structures are prepared by using silver ink printed on polystyrene substrates. Pre-strained polystyrene films, widely known as 'Shrinky Dinks', have become popular for self-folding designs due to their low-cost and easy processibility. The pre-strained polystyrene film can shrink up to 55% along the *XY* plane, which makes it a very good active material for self-folding designs. As shown in figure 1, the principle is that with silver ink trace printed on one side of the polystyrene film, the joule heat generated through current will introduce difference in shrinking ratio along the thickness of the film, thus generating the folding behavior. Thermal analyses have been performed to guide the design of the structure. The current and unit resistance of the printed ink traces are critical in determining the folding behavior. An angle lock design is used to accurately control the folding angle to satisfy specific applications. Time to initiate the folding as well as sequential folding is also discussed. In the experimental results, we demonstrate, from silver ink printed polystyrene films, a self-folding lock is fabricated by using the sequential folding and a 3D antenna is fabricated with two sets of controllable folding angles. More test cases and folding videos can be found in the supporting information of the paper is available online at stacks.iop.org/SMS/26/085040/mmedia.

2. Design concept

2.1. Folding behavior of polystyrene film activated by current

Heat conduction is an important factor affecting the folding process based on polystyrene films. The governing equations regarding the thermal analysis are shown below. Figures 1(a) and (b) show the schematic diagram and the image of the self-folding behavior of the polystyrene film triggered by the current through silver ink trace. With the models shown in figures 1(d) and (e), the heat conduction problem can be regarded as semi-infinite surface heat conduction. The assumptions in the analysis are that the temperature field is the same along the *Y*-axis, and the surface diffusivity can be ignored since it is much smaller than the heat conduction through the *Z*-axis (the thickness direction). Equation (1) is the thermal conduction differential equation for the semi-infinite surface heat conduction, where *T* is the temperature

field, t is the time, a is the thermal diffusivity of the film, $b = \frac{2a}{c\rho h}$ is the heat diffusion coefficient, c is the specific heat capacity of the material, ρ is the density, h is the thickness of the film. Since the surface diffusivity can be ignored, the term $-bT$ can be removed, equation (1) becomes equation (2). By solving the equation, we have the temperature distribution function as shown in equation (3), where Q_0 is the joule heat generated by the circuit, λ is the thermal conductivity of the film, L is the length of the silver trace, r is the distance between the target point and the heating source $r = \sqrt{x^2 + z^2}$.

$$\frac{\partial T}{\partial t} = a\left(\frac{\partial^2 T}{\partial x^2} + \frac{\partial^2 T}{\partial z^2}\right) - bT, \tag{1}$$

$$\frac{\partial T}{\partial t} = a\left(\frac{\partial^2 T}{\partial x^2} + \frac{\partial^2 T}{\partial z^2}\right), \tag{2}$$

$$T = \frac{Q_0}{4\pi\lambda L t}\exp\left(-\frac{r^2}{4at}\right), \tag{3}$$

$$\begin{aligned} T = \sum_{i=1}^{n} T(r_i) = \frac{Q_s}{4\pi\lambda L t}\Bigg[&\exp\left(-\frac{{r_1}^2}{4at}\right) \\ &+ \exp\left(-\frac{{r_2}^2}{4at}\right) + \ \ldots\ + \exp\left(-\frac{{r_n}^2}{4at}\right)\Bigg] \\ = \frac{Q_s}{4\pi\lambda L t}\int_0^W &\frac{-2x^*}{4at}\exp\left(-\frac{x^{*2} + z^2}{4at}\right)\mathrm{d}x^*. \end{aligned} \tag{4}$$

Here two models could be used regarding the heating source, the single point model and the multi-point model. In the single point model, the heating source is regarded as a concentrated single point. Equation (3) is the expression of the temperature field under single point model. In multi-point model, the ink trace is regarded as several heating points. The heat is divided uniformly along the width of the ink trace, so $Q_0 = n \times Q_s$, where Q_s is the divided heat regarding the n heating sources. So in the multi-point model, the temperature for a certain location becomes the sum of each heating sources, expressed in equation (4), where $r_1 \ldots r_n$ is the distance between the target location and the corresponding heating sources, denoted as r^* $(r^{*2} = x^{*2} + z^2)$ in figure 1(e), W is the width of the printed silver ink trace. The isothermals could be drawn based on equation (4) as shown in figure 1(e), from which we can see the locations with the similar temperature.

For a thin silver trace (i.e. w is small), we can use the single point model to guide the experiment design . Since joule heat $Q_0 = I^2R \times t$, by plugging this into equation (3), we have equation (5).

$$T = \frac{I^2R}{4\pi\lambda L}\exp\left(-\frac{r^2}{4at}\right)T = \frac{I^2R}{4\pi\lambda L}\exp\left(-\frac{r^2}{4at}\right). \tag{5}$$

We can get the max temperature in the single point model as $T_{\max} = \frac{I^2R}{4\pi\lambda L}$. In order to trigger the folding behavior, the max temperature should be higher than the glass transition temperature of the film, i.e. $T_{\max} > T_g \approx 102\ ^\circ\mathrm{C}$. We can also get the temperature of the bottom surface location ($x = 0$, $z = h$) for a certain amount of time t_*, $T_{\text{yield}} = \frac{I^2R}{4\pi\lambda L}\exp\left(-\frac{h^2}{4at_*}\right)$. According to the thermal model, this location is the point with the highest temperature on the bottom side. In order to keep the shape, this temperature should be smaller than the soften temperature 120 °C. Thus we have $T_{\text{yield}} < T_{\text{soft}} \approx 120\ ^\circ\mathrm{C}$. The values of $T_{\max}$ and T_{yield} can be used to guide the setting of current I. The shrinking ratio of the film s is determined by the temperature $s = f(T)$ and the folding angle α is determined by the shrinking ratio of the structure $\alpha = g(s)$. Hence the folding angle α is determined by the factors that affecting the temperature, which is (I, R, L, t), the current I, the unit resistance R/L, and the time t.

2.2. Materials and experiments

The polystyrene film used in this study is INK JET Shrink Film (Clear) from Grafix. The film is used for material coating and possesses uniform shrinking behavior. The silver ink material is PELCO Conductive Silver Paint from TED PELLA Inc. The silver ink is printed on top of the polystyrene film using an in-house developed direct writing system (figure 2), where an extruder is mounted onto a TinyG computer numerically controlled (CNC) stage, the motion of the stage defines the contour of the printing pattern. Printing parameters such as feed rate, printing speed, diameter of the nozzle tip and nozzle height can be adjusted for ink traces with various thickness and width. For the folding angle measurement along increased current, an angel gauge is used to measure the folding angle, the accuracy of the measurement is 2.5°.

2.3. Printing procedure

The schematic diagram in figure 2 shows the printing process. The circuit design is first drawn using software in the form of two-dimensional (2D) sketch, then the sketch is turned into a machine code called G code that can be used by the CNC printing stage. A software interface called Chilipeppr is used to upload the G-code into the TinyG controller. The silver ink is filled in the syringe and the distance between nozzle tip and polystyrene film is adjusted before printing. The printing speed is controlled by the software and goes along the programmed path. For designs with circuit on both sides, we need to flip the polystyrene film and print on the other side. After the printing process, the film is cut according to the designed shape using scissors or a CNC router with a diamond cutter. For the angle lock design, the lock features are also cut and a steel cube with 90° standard angles is used to bend the film related to the locks up into 90°. For the circuit pins, holes on the polystyrene film were added by a hand drill and connect the wires onto the film. A microcontroller was used to connect the other ends of the wires to provide the current to each hinge sequentially, thus achieving the desired folding procedure.

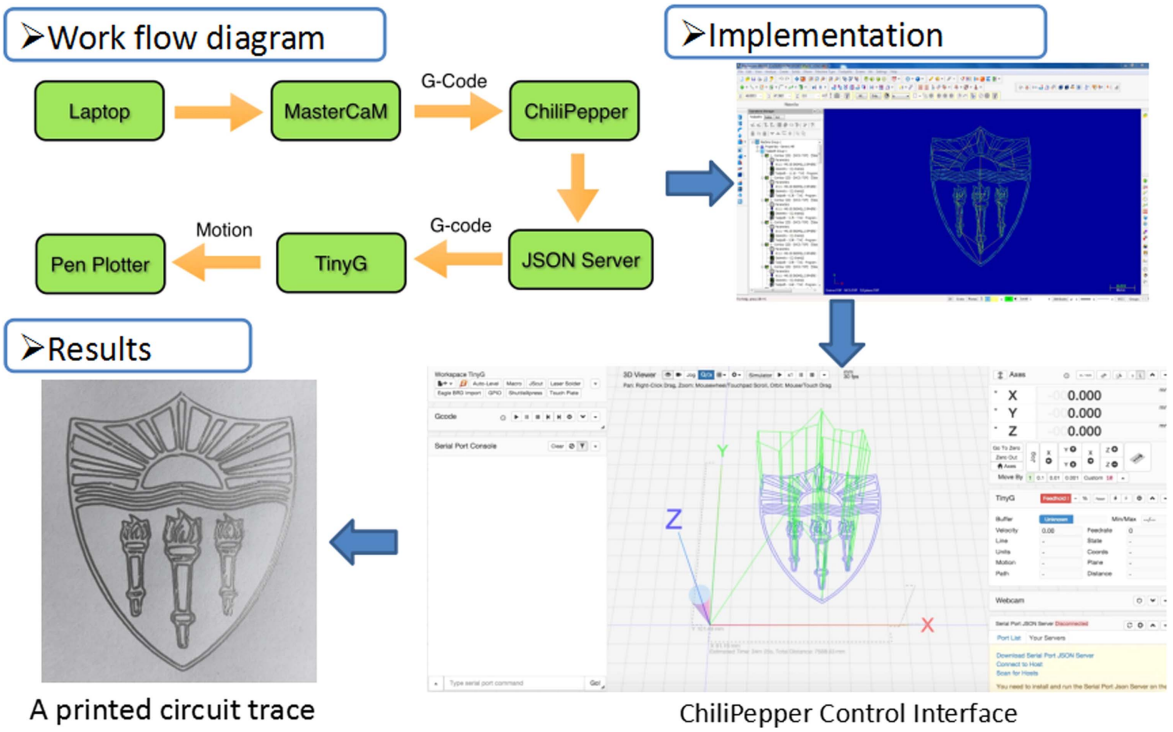

Figure 2. The printing process of a circuit trace of USC logo.

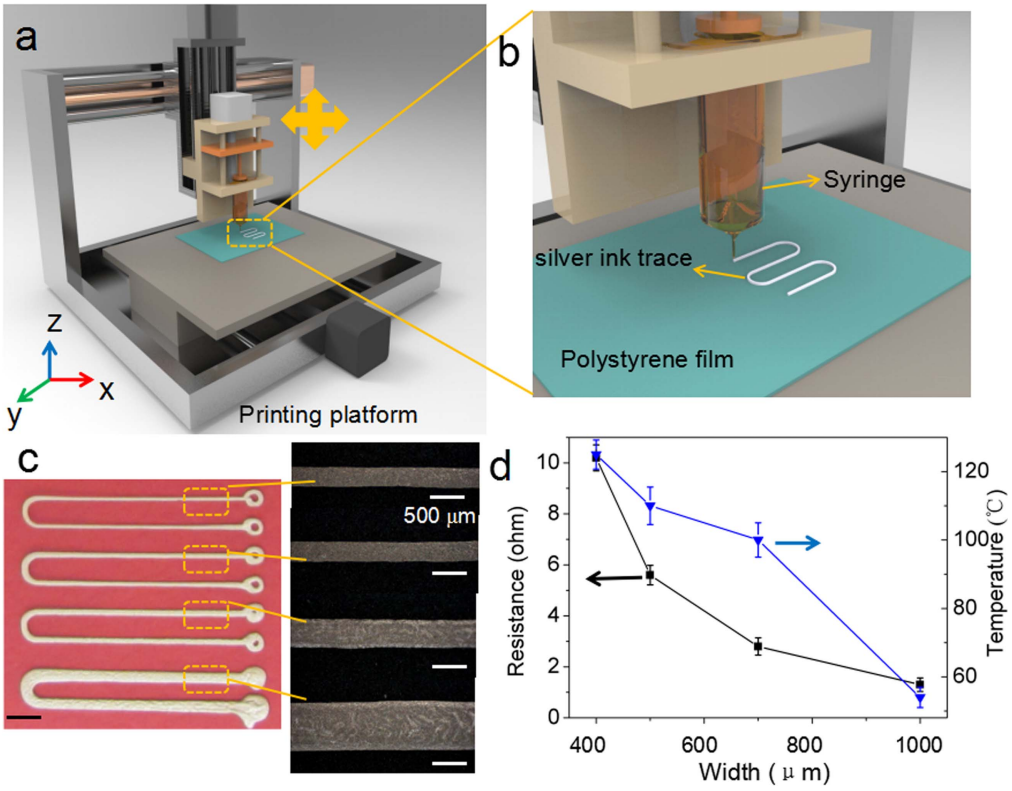

Figure 3. (a) Schematic of the printer used for the silver ink trace on polystyrene substrate; (b) inset highlighting the syringe and silver ink trace controlled by software; (c) the printed ink trace with various width and shapes with corresponding optical microscope images showing the microstructure; (d) resistance and temperature after the current (0.8 A) activated changes with the width of the silver ink trace.

2.4. Printing of silver ink traces on polystyrene films

The diagram shows the printing platform for the silver ink trace on polystyrene film. The shape of the silver ink trace is controlled by G code and printed by a CNC printing stage. The width and thickness of the silver ink trace are controlled by the height of the nozzle and the printing speed. When voltage is applied on the ink trace, the temperature on the polystyrene film will increase. The results in figure 3(d) show that both the resistance and temperature decrease with the silver trace width. The resistance decrease is due to the increment of width according to the formula $R = \rho l/s$, $s = Wd$, where ρ is the resistivity of silver ink trace, l is the length and s is the area of section, W is the width and d is the thickness. The heat (H) of current applied on the silver ink trace will increase with an increased resistance attributed to the formula: $H = I^2Rt$. The heat applied on the polystyrene film activates the shrinkage of the film and leads to self-folding behavior. In this way, the folding of the polystyrene will be controlled by the ink trace design; based on it various applications are studied as follows.

3. Results and discussion

3.1. Printing parameters optimization

There are several parameters in the printing process need to be identified to optimize the printed circuit trace quality. These parameters include the nozzle size, printing speed, extrusion speed, the distance between nozzle and printing surface (called nozzle height in the paper). The nozzle size of the extruder needs to be selected because the extrusion will not be smooth if the nozzle size is too small. The nozzle may even not be able to extrude any materials due to the high pressure drop inside the small nozzle. At the same time, if the nozzle size is too large, the printed trace will be wide and the extrusion resolution will be low. Based on our experiments, nozzle with 279 μm inner diameter is selected to be the most suitable. Using the nozzle the best printing resolution that has been achieved is between 350 and 500 μm as shown in figure 4(a). The ink material used in our study is PELCO Conductive Silver Paint. The material has good conductivity as well as mechanical strength.

In addition to the linear stage moving speed and the syringe extrusion speed, nozzle height affects the printed trace width and the resistance of the trace. One critical property of the conductive traces that needs to be well controlled is the resistance per unit length. Figure 4(b) shows a model of the syringe extruder for the analysis of the conductive ink extrusion process.

When the extruder starts to print the circuit trace, the ink is pushed out by the syringe through the nozzle. There is a compression of the paste material inside the syringe denoted as the volume decreased inside the syringe ΔV in the amount of extrusion time Δt. Hence

$$\Delta V = \pi \frac{\Phi_1^2}{4} \times V_1 \times \Delta t. \tag{6}$$

Assume the printed trace has uniform width and thickness. The volume that is extruded out of the nozzle is:

$$\Delta V' = V_3 \times w \times d \times \Delta t. \tag{7}$$

Denote the density of the ink material inside the syringe as, and the density of the ink material out of the nozzle as. We have:

$$\rho_1 \Delta V = \rho_2 \Delta V'. \tag{8}$$

Based on equations (6)–(8), we have:

$$\frac{1}{w \times d} = \frac{V_3}{V_1} \times \frac{\rho_2}{\rho_1} \times \frac{4}{\pi \Phi_1^2}. \tag{9}$$

To calculate the resistance over length, the resistance equation is:

$$R = \rho \frac{L}{w \times d}. \tag{10}$$

Hence we have:

$$\frac{R}{L} = \rho \times \frac{1}{w \times d} = \rho \times \frac{V_3}{V_1} \times \frac{\rho_2}{\rho_1} \times \frac{4}{\pi \Phi_1^2} \tag{11}$$

in which, is the resistivity of the ink material.

From equation (11), we can see that the resistance per unit length of the printed trace is positively related to the feed rate of because we know the density ratio of the ink material $\frac{\rho_2}{\rho_1}$ is changing due to the pressure change within the syringe.

A validation experiment has been performed to study the relationship between the resistance per unit length and the feed rate. Figure 4(c) shows the experimental result. A positive relevant relationship can be identified from the plot with two different functions for large and small $\frac{V_3}{V_1}$ values.

To study the effect of nozzle height, different values of nozzle height are tested using the setup. It is found that the nozzle height should be selected properly. That is, if the nozzle height is too small, the ink material is squeezed during the printing process, which leads to a large printed width of the trace as shown in figure 4(d). However, if the nozzle height is too large, the extruded material will first grow and accumulate on the nozzle tip since the viscosity of the silver ink is high. The accumulation process will continue until it becomes big enough to touch and land on the printing surface. Consequently, the printed ink trace is non-uniform as shown in figure 4(d). In our study, we select nozzle height to be 200 μm. The accordingly printed ink trace is thin and uniform as shown in figure 4(d).

Polystyrene substrates are pre-strained due to stretching and rapid cooling in the manufacturing process. When the temperature rises above its glass transition temperature, the material will shrink along the XY plane and expand in thickness. This shrinking ratio of the film is directly determined by the temperature. Figure 5(a) shows the relationship between the shrinking ratio and temperature. The film will start to shrink at around 102 °C (T_g). Then the shrinking ratio will continue to increase until the temperature reaches around 120 °C, where the material starts to become soft and the shrinking ratio becomes stabilized. The shrinking of the sample is shown in figure 5(a). For temperatures between 102 °C and 120 °C, the shrinking ratio

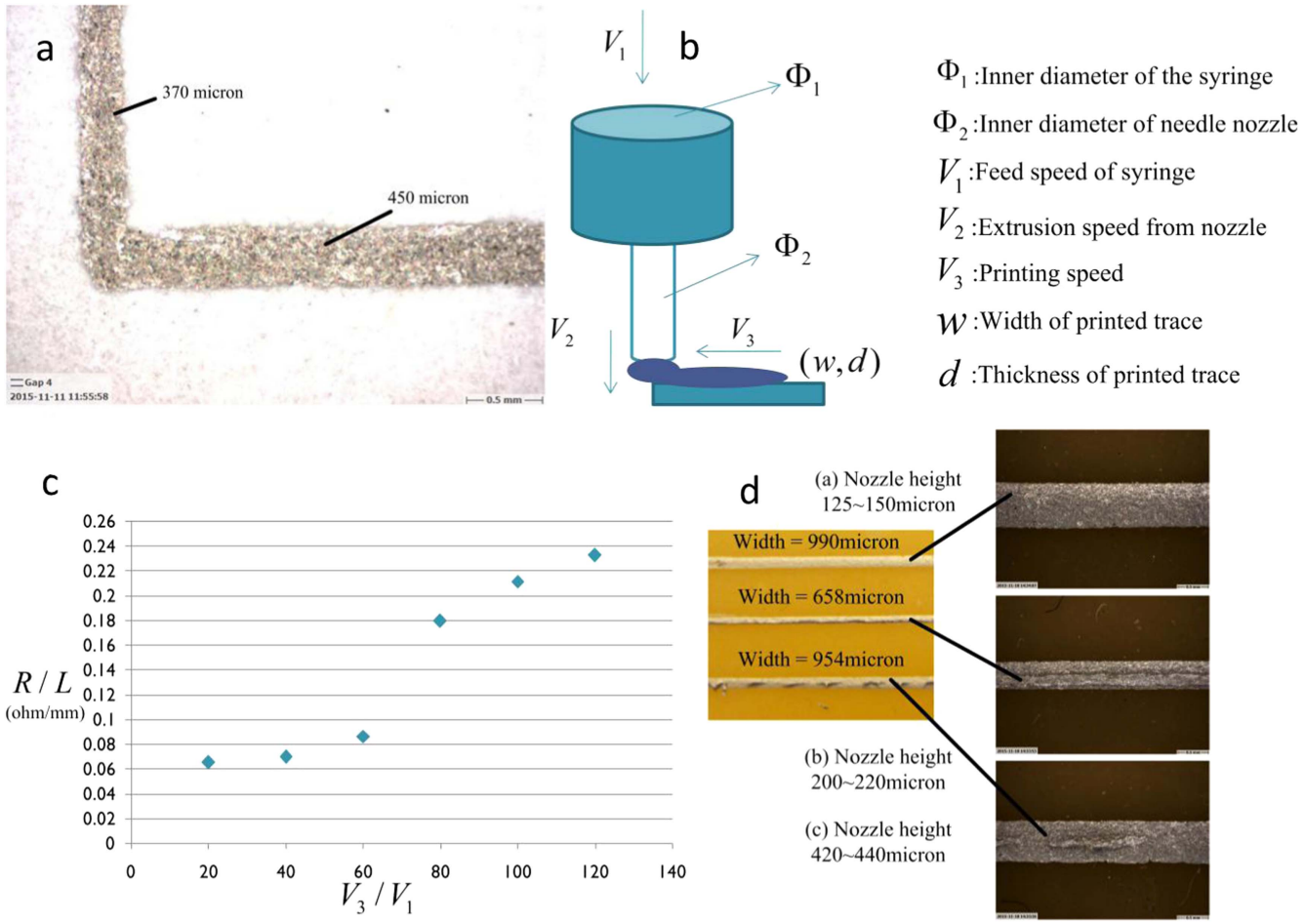

Figure 4. (a) Printed ink trace; (b) the ink extrusion model; (c) experimental results on resistance per unit length versus feed rate; (d) printed trace width versus nozzle height.

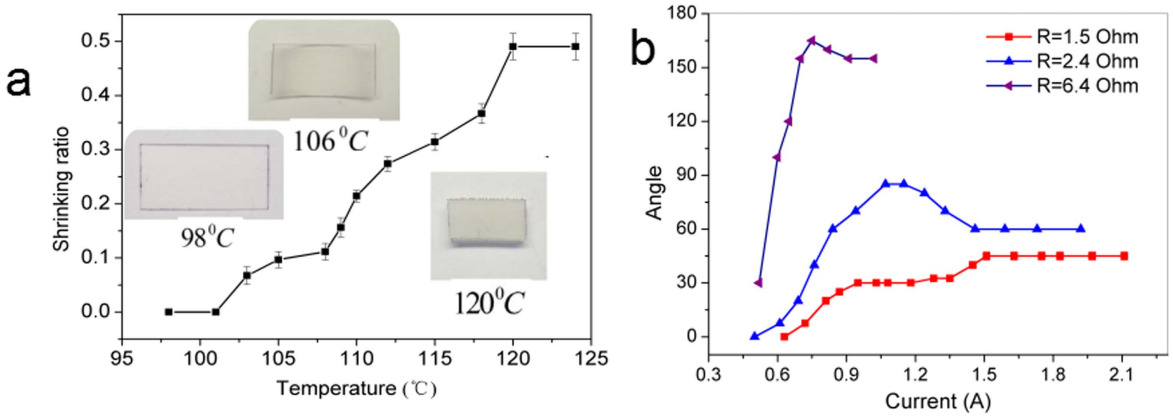

Figure 5. Folding behavior of the self-folding structure. (a) Shrinking ratio versus temperature, insert pictures show the shrinking process of a polystyrene sheet; and (b) folding angle versus current.

becomes fixed. Heat is needed to trigger the phase transition; however, the heat transfer between the environment and the film will become stable with a fixed temperature setting so that the energy absorbed by the film is fixed. Once the heat is large enough for the entire film to go through a phase transition, the film becomes soft. Electrically conductive silver ink serves as the heat source to the film, which causes a shrinking ratio difference along the *Z*-direction in the film. By adjusting the resistance and the current applied on the silver ink trace, different film temperatures along the thickness are achieved, which generate different folding angles as shown in figure 5(b).

A set of tests have been done to study the relationship between the folding angle and the current, as well as unit resistance. The length of samples is 10 mm. Figure 5(b) shows the folding angles for various samples with different resistance and current. In this test, the amount of time is long

enough for the folding angle to become stable. The results show that the folding behavior starts at a lower current for a higher resistance. The folding angle will reach a maximum value and then, with the increase of current, the angle will bounce back. This is because the heat transfer leads to a temperature increase in the film which triggers the shrinkage first on the top side of the film. Hence the hinge will fold. When the temperature keeps increasing and the shrinkage reaches the bottom side of the film, the folding angle will start to bounce back due to the decreased difference on shrinkage ratio along the film thickness. It will reach a stable folding angle at certain current value when the top and bottom sides stop shrinking.

3.2. Accurate folding by a novel angle lock design

In order to accurately control the folding angle of a designed structure, an angle lock design using the polystyrene film is studied. As shown in figure 6, the angle lock design is two blocking structures that align with the ink trace. When the hinge folds, the two blocks will contact and stop the structure from further folding. The angle lock design could be used to constrain the maximum folding angle allowed for a certain parameter setting. Parameters that affect the blocking angle are shown in figure 6(c), including the height of the two blocks h and s_2, the width of the gap $s_3 + d$ between them, and the length of the extended block s_1. The angle lock design has two pieces of blocks, denoted as the first block (in blue color) and the second block (in yellow color) in the following analysis. They will contact with each other during the folding process to constrain the maximum folding angle that is allowed as shown in figure 6(a). It is shown that the folding angle is related to these parameters. Three special cases to achieve different ranges of folding angles are discussed in figures 6(b)–(d), respectively. The parameters can be adjusted to achieve different folding angles.

In the first case, the extra material is added on one block so that the other block can contact it in a smaller angle with the range of 0°–45° (figure 6(b)). The relationship between the extended length s and the folding angle α can be seen in figure 6(b). In the second design, by adjusting the height of the second block, larger folding angles could be achieved between 45° and 90°. The relationship between the height of the second block and the folding angle is shown in figure 6(c). In the third design, a gap between the first block and the folding axis is added. By adjusting the length of the gap, various folding angles ranging from 45° to 135° can be achieved. The relationship between the gap and the folding angle could be seen in figure 6(d). The idea of using angle lock is to constrain the folding angle before its bouncing back. Another benefit is that the angle lock design will have little effect on the folding angle if an error is added to the lock. As shown in figure 6(e), compared with an accurate 90° folding of the angle lock, an error of θ is added to the yellow lock. The result show that it will lead to an error of $\theta/2$ to the folding angle. For the blue angle lock, it will have no effect on the folding angle in a proper range (red dot line in figure 6(e)). The results show that the error is reduced by half based on our angle lock design. Figure 7(f) show the picture of different folding angles with the related angle block design is shown in figure 6(c1–3) , respectively. The comparison shows that the experimental values of folding angles fit well to the theoretical values (figures 7(c)–(e)). This indicates that the folding angle could be accurately controlled by the designed angle lock.

3.3. Sequential folding

Sequential folding can be designed based on the current induced folding method. Two different approaches are studied. The first approach is folding using ink trace in various unit resistance in a single circuit. The second approach is folding using multiple circuits with uniform ink traces. As shown in figure 8(a), ink traces with various unit resistance can be achieved by adjusting printing parameters such as printing speed, nozzle height and material feed rate. Based on equation (3), it is demonstrated that with the same current amplitude in a single circuit, the edges with larger unit resistance will reach the glass transition faster than the ones with lower unit resistance and start to fold first. In the designed sample as shown in figure 8(a), the length of each edge is 18 mm, the resistance for three varied ink traces are 1.7 Ω, 1.0 Ω and 0.6 Ω, respectively. The trigger current for each edge is tested as 0.82 A, 1.11 A, 1.40 A, respectively. By adjusting the current to different ranges, sequential folding of the design is realized. This method gives us an easy way to fabricate the sequential folding structures by using a single circuit.

The second approach is to use multiple circuits to trigger the folding in different sequence. Figures 8(b) and (c) show a structure that locks itself using sequential folding. There are three folding hinges in the structure and the features are designed for locking at the two ends. On piece on the left side of the structure acts as the ‘lock’ and the piece with an opening on the right side is the ‘handle’. In the folding process, the piece with the ‘lock’ will fold first, then the ‘handle’ piece folds to enable the ‘lock’ to go into the ‘handle’. Finally the ‘lock’ piece will fold and lock the structure itself. This type of structure cannot be made other than the designed sequential folding because the accurate control of the folding time is needed in order for the ‘lock’ to precisely go into the ‘handle’, and to subsequently be folded down to secure the two pieces together.

3.4. Self-folding origami structure design

Using both uniform self-folding as well as sequential self-folding approaches, many applications become viable. We demonstrate self-folding 3D electronic components, antennas, and self-folding origami designs. Figure 9 shows a demo case similar to an ‘inverted F’ antenna as well as ‘USC’ lettered circuit boards. This structure is used to demonstrate the feasibility of printing antennas on the selected foldable substrate. The self-folding structure is composed of two types of circuits. One of them is the circuit that provides functionality such as the ‘inverted F’ antenna portion in the design. The

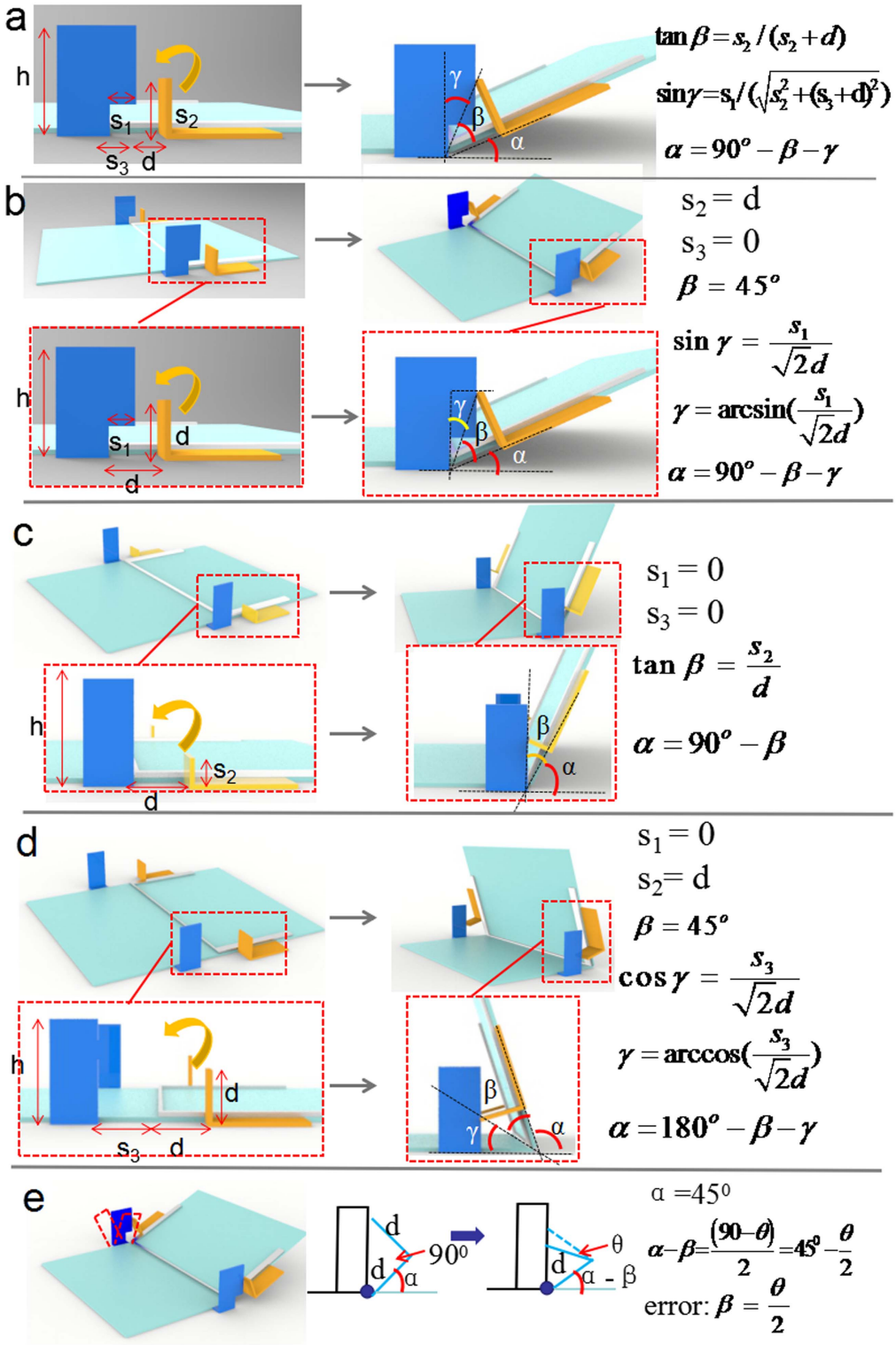

Figure 6. Angle lock design and its variation for angle control. (a) Angle lock design variations, the folding angle is related with five parameters: *h*, *s*1, *s*2, *s*3, *d*. Illustration of three special cases for the relationship between folding angle and the design parameters for different ranges: (b) 0°–45°, (c) 45°–90°, (d) 45°–135°; and (e) error analysis of the angle lock.

other is folding circuits, which are added specifically for self-folding purposes. The self-folding circuits are also easier for the transportation of the designed structures since it can remains in 2D and can turn into 3D shapes after it is in use.

The other is the folding circuits, which are added specifically for the aforementioned self-folding purpose. The folding circuits are printed either on the same side of the functional circuits, or on the other side to minimize the potential

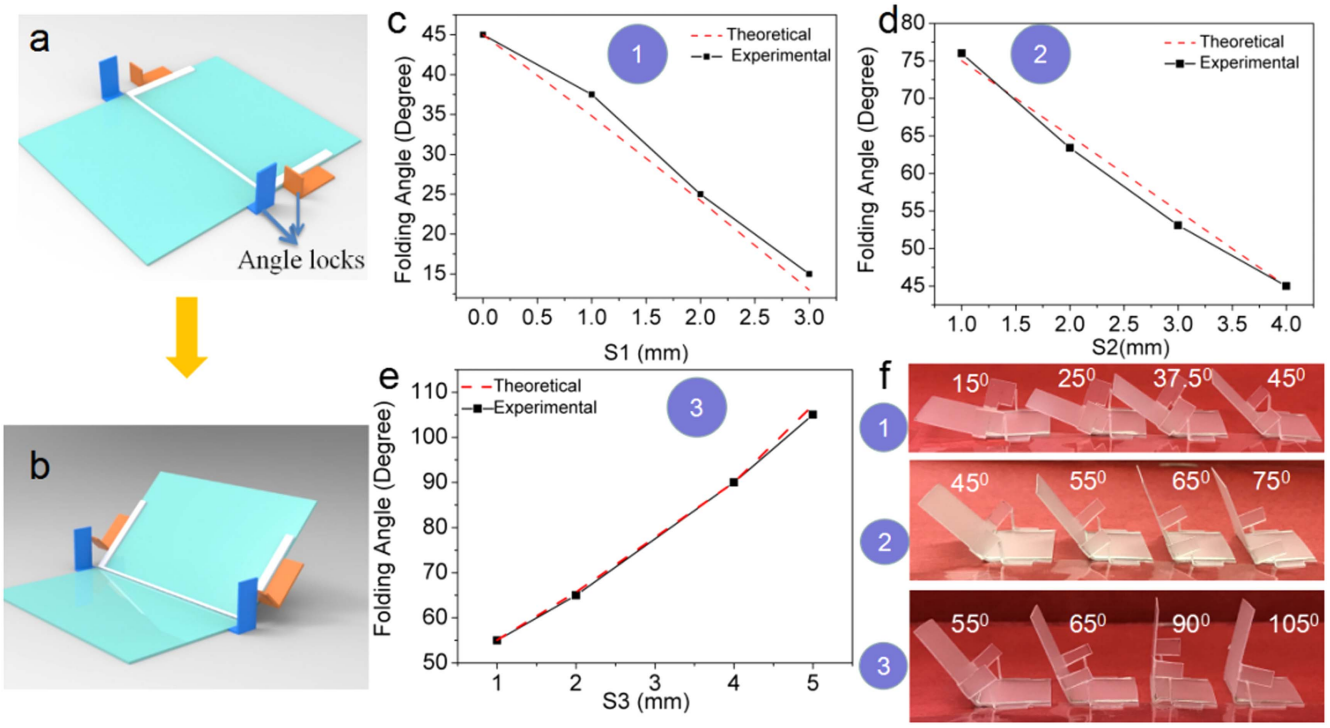

Figure 7. Self-folding structure with angle lock control design. (a) Schematic diagram of angle locks design and after the folding (b); (c), (f1) angles ranging from 0° to 45°; (d), (f2) angels ranging from 45° to 90°; and (e), (f3) angles ranging from 45° to 135°.

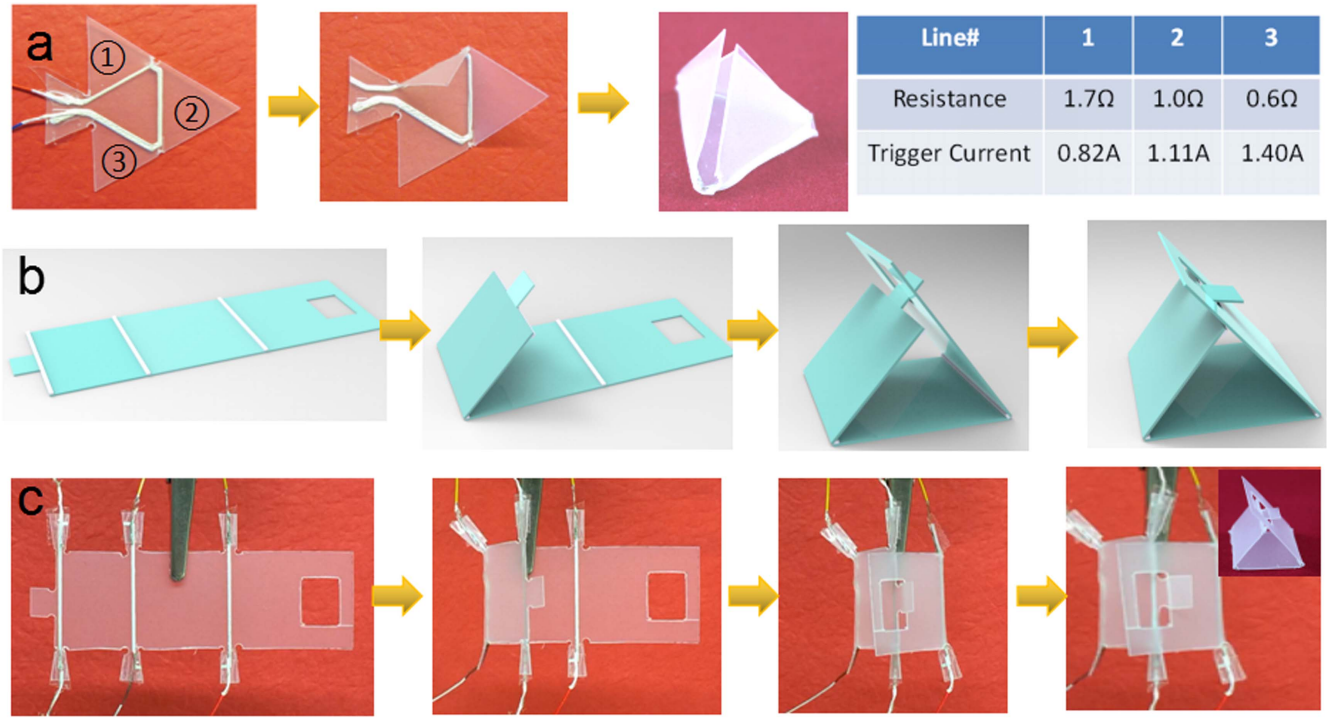

Line#	1	2	3
Resistance	1.7Ω	1.0Ω	0.6Ω
Trigger Current	0.82A	1.11A	1.40A

Figure 8. Sequential self-folding structure. (a) A pyramid structure design with a sequential folding by using different resistance in different areas for one silver ink trace shown in the table; (b), (c) schematic diagram and images show sequential folding process of a lock structure by multiple circuits design.

interference and to fold the structure in different orientations. As shown in the Origami crane model in figures 9(b) and (c), multiple circuits folding were used with the silver ink trace on both sides. Firstly, the body of the crane was folded by triggering the silver ink trace on the front. Then the wings and head were folded by triggering the backside silver ink trace. The structure uses multiple circuit designs as mentioned before so that complex shapes can be achieved with sequential steps

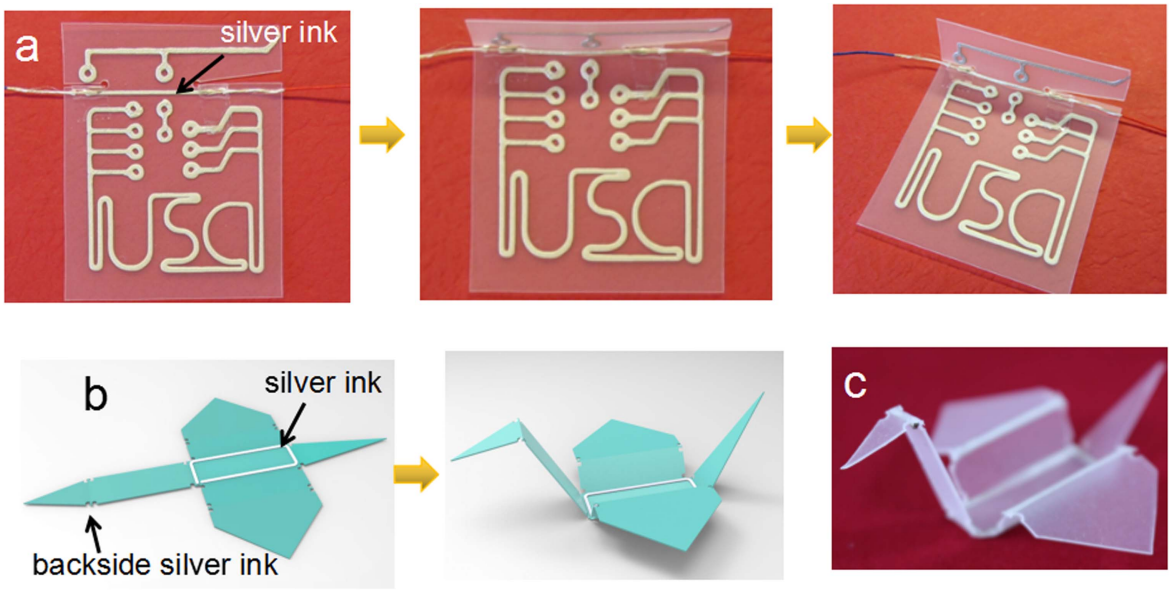

Figure 9. Self-folding origami structures. (a) An 'inverted F' antenna demo case; and (b) origami crane model using multiple circuits folding.

of self-folding. The folding current for each hinge is set using the folding angle curve as shown in figure 5.

Self-folded circuit designs have much potential in applications such as 3D antennas, robotics and wearable devices. Antennas currently take up a large volume since the devices are using 2D circuit boards. The self-folding circuits allow for easier transportation since their 2D shape is maintained and only activated to a 3D structure during its use. In addition, customized antenna arrays with directed radiation patterns can be realized by controlling each antenna element's folding position. For example, either sectorial or omnidirectional patterns can be formed by selectively folding up one or more tabs on which each antenna element resides. When electronic switches are incorporated to the structure, each antenna element can be selectively turned on or off to provide reconfigurability and flexibility. The results will change how phased arrays are perceived for future applications. Conventional planar designs often use multiple antennae to achieve the required functionality and flexibility, which comes with the disadvantages of being costly and bulky for overall communications systems. The 4D foldable antennas overcome these shortcomings and enabling replacement of multiple elements with a single antenna.

To make the self-folding structure to be easily controlled, circuit design layout is studied to make the design neat and clean. Several designs have been tried to realize the design of multiple hinge folding in one structure and discussed in figure 10. The results show that the 'jump' from the back design performs well. To make the connection between the self-folding structure and the controller easier, circuit design layout is studied to make the connection neat and clean. Several ways have been tried as shown in figure 10 to realize the design of multiple hinge-based folding in one structure. To realize the folding along multiple hinges in one structure, the circuit has to be designed so that each hinge can be folded separately by the controller. Figure 10(a) shows a hand model with parallel connection of the circuit hinges. It turns out that the difference of the resistance between the hinge portion and the connection portion is not big enough. The first hinge will always short the other hinges and block their folding. Hand model in figure 10(b) uses a serial connection of each hinge circuit so that there is current passing through the hinge portion. Hence all the hinges in the structure will be folded. However, another problem arises, that is, since the circuit traces will all generate heat, the portion with denser circuit lines will accumulate more heat than the others, which will cause the polystyrene film to deform and generate distortion. Figure 10(c) is a decoupled circuit design, the circuits will share one edge, while the others are separated. In this way the hinges are separated and will not affect each other's folding behavior. However, the portion of the film that has parallel circuit traces will not fold for the bottom hinge since there is extra material left on the hinge portion. To solve the constraint problem introduced by the extra material that may stop the hinge from folding, we came up with two other designs as shown in figures 10(d) and (e). The one in figure 10(d) uses a sharp corner at the hinge portion to decrease the amount of extra material on the hinge. However, there is still heat generated at that corner that will cause the film to shrink and melt. Also, the structure is not easy to extend to more hinges since the corner needs to become larger and larger with more hinges to pass through it. The result in figure 10(e) presents another approach by using a jumping mechanism. The two circuits are decoupled by allowing the outmost circuit to pass across the hinge by using pin holes and conductive ink connections from the back side of the film. This design can be used for more hinges. One limitation is that the folding sequence has to be from outmost to the bottommost to avoid

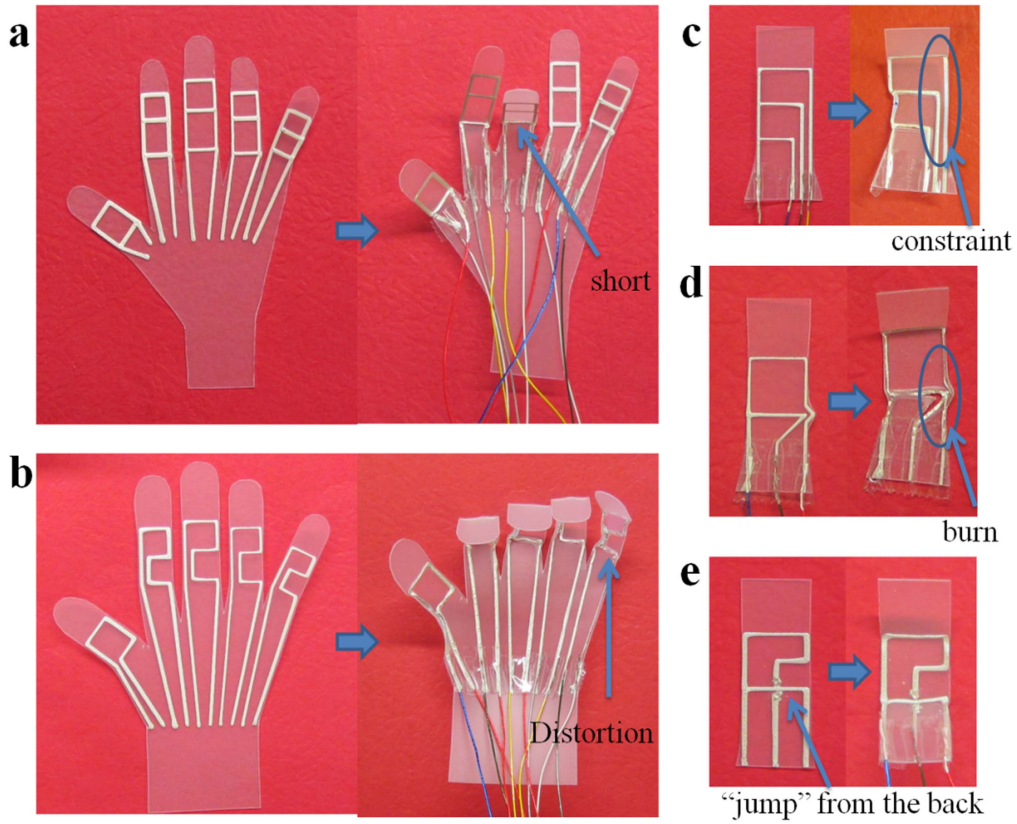

Figure 10. Circuit design layouts for multiple hinge structures. (a) A parallel circuit design; (b) a serial connection circuit design; (c) decoupled circuit design in parallel layout; (d) sharp corner decoupled circuit design; and (e) decoupled circuit 'jump' design.

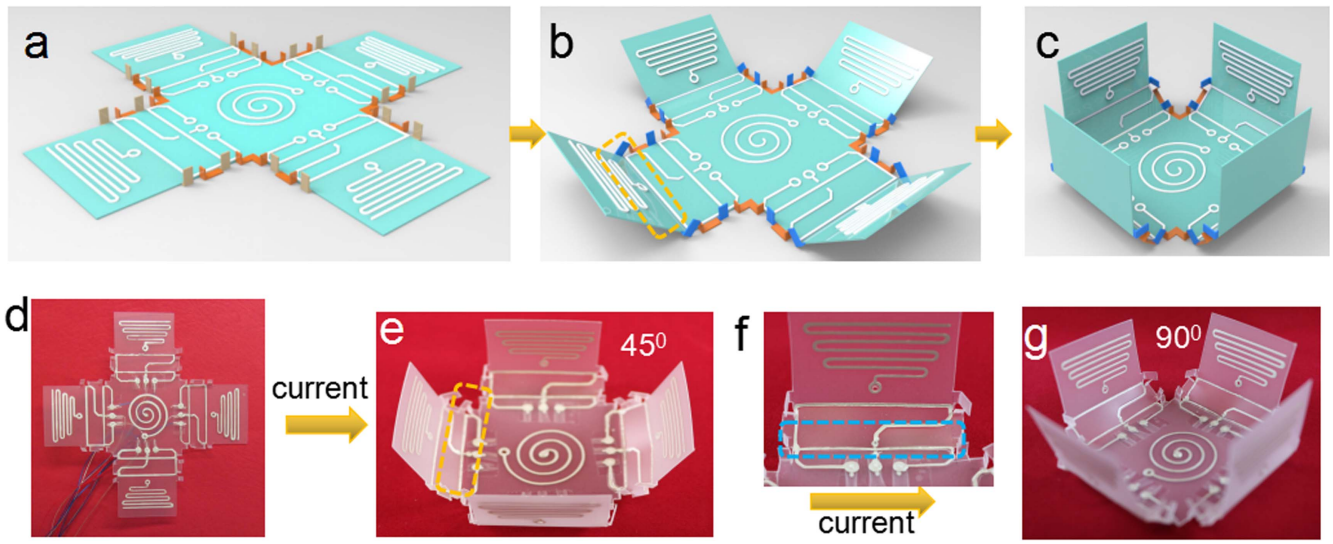

Figure 11. A self-folding antenna structure. Schematic diagram (a)–(c) and pictures (d)–(g) show an 'inverted F' antenna test case using multiple sequential folding.

the potential damage of the outmost circuit when the bottommost hinge is folded. This approach is used in the 3D antenna design (refer to figure 11).

A two-phase 3D antenna design implemented using the sequential folding method and angle lock features developed in this study is shown in figure 11. The antenna is first in a 2D layout and can be folded into different 3D layouts to enhance the signal transmission. A decoupled 'jump' design is used for the multiple-hinge folding in the antenna. The designed 3D antenna has two phases. In the first phase, the four petals of the antenna will fold along the first outmost hinge to form a 45° folding (figure 11(e)). In the second phase, the four petals will

continue to fold along the second hinge for another 45°, so the total folding degree of the antenna petals are 90° (figure 11(g)). More hinges can easily be added to each petal for more folding angles, and the folding angle of each hinge can also be easily changed. The multi-phase design of the antenna that can transform its shape could achieve much more functionality by dynamically changing the antenna configurations.

4. Conclusion

In this study we have demonstrated a design and fabrication method to self-fold polystyrene substrates using electrically triggered silver ink traces. To control the self-folding process, thermal models are established to analyze the temperature field of the structure. Key factors that affect the folding behavior are identified including current and unit resistance of the printed ink traces. Additionally, folding angles are calibrated with current and unit resistance. An angle lock design using the polystyrene film has been developed to accurately control the folding angle of a hinge in the self-folding structure. Programmable structures such as a lock and a 3D antenna have been achieved to demonstrate the feasibility and potential applications of the method. Our method provides a simple and low-cost way to achieve the sequential folding with accurate folding angle control. Finally, we have introduced a new path for future study of electronic components that can dynamically change shapes to allow entirely new applications.

Acknowledgments

We acknowledge the support of Northrop Grumman Institute of Optical Nanomaterials and Nanophotonics (NG-ION^2) at USC.

Author contributions

DPD developed the 4D printing system, DPD, YY and Professor YC conducted the preliminary experiments, and contributed to the development of 4D printing system and manuscript preparation. XL and JT contributed to the concept development and manuscript. All authors reviewed the manuscript.

Competing financial interests

The authors declare no competing financial interests.

ORCID

Jesse Tice https://orcid.org/0000-0001-9920-2507

References

[1] Davis D, Chen B, Dickey M D and Genzer J 2016 Self-folding of thick polymer sheets using gradients of heat *J. Mech. Robot.* **8** 031014
[2] Miyashita S, Onal C D and Rus D 2015 Multi-crease self-folding by global heating *Artif. Life* **21** 398–411
[3] Deng D and Chen Y 2015 Origami-based self-folding structure design and fabrication using projection based stereolithography *J. Mech. Des.* **137** 21701
[4] Han D *et al* 2015 Moisture-responsive graphene paper prepared by self-controlled photoreduction *Adv. Mater.* **27** 332–8
[5] Terashima T, Sugita T and Sawamoto M 2015 Single-chain crosslinked star polymers via intramolecular crosslinking of self-folding amphiphilic copolymers in water *Polym. J.* **47** 667
[6] Deng T, Yoon C, Jin Q, Li M, Liu Z and Gracias D H 2015 Self-folding graphene-polymer bilayers *Appl. Phys. Lett.* **106** 203108
[7] Guan J, He H, Hansford D J and Lee L J 2005 Self-folding of three-dimensional hydrogel microstructures *J. Phys. Chem.* B **109** 23134–7
[8] Fernandes R and Gracias D H 2012 Self-folding polymeric containers for encapsulation and delivery of drugs *Adv. Drug. Deliv. Rev.* **64** 1579–89
[9] Gladman A S, Matsumoto E A, Nuzzo R G, Mahadevan L and Lewis J A 2016 Biomimetic 4D printing *Nat. Mater.* **15** 413
[10] Ge Q, Dunn C K, Qi H J and Dunn M L 2014 Active origami by 4D printing *Smart Mater. Struct.* **23** 094007
[11] Kwok T, Wang C C L, Deng D, Zhang Y and Chen Y 2015 4D printing for freeform surfaces: design optimization of origami structures *J. Mech. Des.* **137** 111413
[12] Mao Y *et al* 2015 Sequential self-folding structures by 3D printed digital shape memory polymers *Sci. Rep.* **5** 13616
[13] Shenoy V B and Gracias D H 2012 Self-folding thin-film materials: from nanopolyhedra to graphene origami *MRS Bull.* **37** 847
[14] Randall C L, Gultepe E and Gracias D H 2011 Self-folding devices and materials for biomedical applications *Trends Biotechnol.* **30** 138–46
[15] Azam A, Laflin K E, Jamal M, Fernandes R and Gracias D H 2011 Self-folding micropatterned polymeric containers *Biomed. Microdevices* **13** 51–8
[16] Guan J, He H, Lee L J and Hansford D J 2007 Fabrication of particulate reservoir-containing, capsulelike, and self-folding polymer microstructures for drug delivery *Small* **3** 412–8
[17] Breger J C, Yoon C, Xiao R, Kwag H R, Wang M O, Fisher J P and Gracias D H 2015 Self-folding thermo-magnetically responsive soft microgrippers *ACS Appl. Mater. Interfaces* **7** 3398
[18] He H, Guan J and Lee J L 2006 An oral delivery device based on self-folding hydrogels *J. Control. Release* **110** 339–46
[19] Kowalewski J, Mahler T, Reichardt L and Zwick T 2013 Shape memory alloy (SMA)-based pattern-reconfigurable antenna *IEEE Antennas Wireless Propag. Lett.* **12** 1598–601
[20] Felton S, Tolley M, Demaine E, Rus D and Wood R 2014 Applied origami. A method for building self-folding machines *Science* **345** 644–6
[21] Ninh C and Bettinger C J 2013 Reconfigurable biodegradable shape-memory elastomers via diels-alder coupling *Biomacromolecules* **14** 2162–70
[22] Hayes G J, Liu Y, Genzer J, Lazzi G and Dickey M D 2014 Self-folding origami microstrip antennas *IEEE Trans. Antennas Propag.* **62** 5416–9
[23] Miyashita S, Meeker L, Gouldi M, Kawahara Y and Rus D 2014 Self-folding printable elastic electric devices: resistor,

capacitor, and inductor *2014 IEEE Int. Conf. on Robotics and Automation (ICRA)* pp 1446–53
[24] Lee D, Seo Y and Lim S 2016 Dipole- and loop-mode switchable origami paper antenna *Microw. Opt. Technol. Lett.* **58** 668–72
[25] Peraza-Hernandez E, Hartl D, Galvan E and Malak R 2013 Design and optimization of a shape memory alloy-based self-folding sheet *J. Mech. Des.* **135** 111007
[26] Felton S M, Tolley M T and Wood R J 2014 Mechanically programmed self-folding at the millimeter scale *2014 IEEE Int. Conf. on Automation Science and Engineering (CASE)* pp 1232–7
[27] Ding Z, Wei P and Ziaie B 2010 Self-folding smart 3D microstructures using a hydrogel-parylene bilayer *2010 18th Biennial University/Government/Industry, Micro/Nano Symp. (UGIM)* pp 1–4
[28] Jamal M, Kadam S S, Xiao R, Jivan F, Onn T, Fernandes R, Nguyen T D and Gracias D H 2013 Bio-origami hydrogel scaffolds composed of photocrosslinked PEG bilayers *Adv. Healthcare Mater.* **2** 1142–50
[29] Stoychev G, Turcaud S, Dunlop J W C and Ionov L 2013 Hierarchical multi-step folding of polymer bilayers *Adv. Funct. Mater.* **23** 2295–300
[30] Pickett G T 2007 Self-folding origami membranes *Europhys. Lett.* **78** 48003
[31] Guo W, Li M and Zhou J 2013 Modeling programmable deformation of self-folding all-polymer structures with temperature-sensitive hydrogels *Smart Mater. Struct.* **22** 115028
[32] Liu Y, Boyles J K, Genzer J and Dickey M D 2012 Self-folding of polymer sheets using local light absorption *Soft Matter* **8** 1764–9
[33] Felton S M *et al* 2013 Self-folding with shape memory composites *Soft Matter* **9** 7688–94
[34] Tolley M T, Felton S M, Miyashita S, Aukes D, Rus D and Wood R J 2014 Self-folding origami: shape memory composites activated by uniform heating *Smart Mater. Struct.* **23** 094006
[35] Deng D and Chen Y 2015 4D printing: design and fabrication of 3D shell structures with curved surfaces using controlled self-folding *Proc. ASME 2015 MSEC* Paper No. MSEC2015-9459, pp V001T02A070 (https://doi.org/10.1115/MSEC2015-9459)
[36] Liu Y, Miskiewicz M, Escuti M J, Genzer J and Dickey M D 2014 Three-dimensional folding of pre-strained polymer sheets via absorption of laser light *J. Appl. Phys.* **115** 204911
[37] Davis D, Mailen R, Genzer J and Dickey M D 2015 Self-folding of polymer sheets using microwaves and graphene ink *RSC Adv.* **5** 89254–61
[38] Lee Y *et al* 2015 Sequential folding using light-activated polystyrene sheet *Sci. Rep.* **5** 16544
[39] Wu J, Yuan C, Ding Z, Isakov M, Mao Y Q, Wang T J, Dunn M L and Qi H J 2016 Multi-shape active composites by 3D printing of digital shape memory polymers *Sci. Rep.* **6** 24224
[40] Ge Q, Qi H J and Dunn M L 2013 Active materials by four-dimension printing *Appl. Phys. Lett.* **103** 131901